THE DEPENDENCE OF FATIGUE CRACK GROWTH ON HYDROGEN IN WARM-ROLLED 316 AUSTENITIC STAINLESS STEEL

Zhitao Wu[1], Kaiyu Zhang[2], Yuanjian Hong[3], Chengshuang Zhou[4], Jinyang Zheng[5,*] and Lin Zhang[6,*]

[1]Institute of Material Forming and Control Engineering, Zhejiang University of Technology, Hangzhou, 310014, China, wzt5880@163.com

[2]Institute of Material Forming and Control Engineering, Zhejiang University of Technology, Hangzhou, 310014, China, 18867545688@163.com

[3]Institute of Material Forming and Control Engineering, Zhejiang University of Technology, Hangzhou, 310014, china, 1207346815@qq.com

[4]Institute of Material Forming and Control Engineering, Zhejiang University of Technology, Hangzhou, 310014, china, zhoucs@zjut.edu.cn

[5]Institute of Chemical Machinery Engineering, Zhejiang University, Hangzhou, 310027, China，jyzh@zju.edu.cn

[6]Institute of Material Forming and Control Engineering, Zhejiang University of Technology, Hangzhou, 310014, china, zhlin@zjut.edu.cn

ABSTRACT

The fatigue crack growth of warm-rolled type 316 austenitic stainless steel was investigated by adjusting rolling temperature and rolling strain in argon and hydrogen gas atmospheres. Warm rolling improved the strength, but did not increase the hydrogen embrittlement susceptibility. The fatigue crack growth rates (FCGR) of warm-rolled 316 specimens tested in hydrogen decreased with increasing rolling temperature, especially 400℃ rolling. The amount of deformation twins decreased with increasing rolling temperature and twining was completely suppressed at 400℃. Therefore, warm rolling can improve the microstructure of dislocations and deformation twins, and then inhibit the formation of α' martensite, which is favorable to reduce the FCGR in hydrogen gas environment.

Keyword: 316 stainless steel, worm-rolling, hydrogen environment embrittlement, deformation twins, α′ martensite

NOMENCLATURE

HEE	hydrogen environment embrittlement	YS	yield strength
FCGR	fatigue crack growth rate	δ	elongation
SSRT	slow strain rate tensile	CT	compact tension
σ	engineering stress	L_0	initial gauge length
L_F	final gauge length	A_0	initial cross-sectional areas
ΔK	stress intensity factor range	UTS	ultimate tensile strength

M_{d30} temperature at which 50% of the microstructure is transformed to martensite by 0.3 true strain

1. INTRODUCTION

It is well known that high-pressure hydrogen can result in a severe deterioration of the mechanical properties of most metallic alloys, such as a marked increase in the fatigue-crack propagation and the

susceptibility of hydrogen embrittlement [1]. Cr-Ni austenitic stainless steel is widely used in high-pressure hydrogen system as hydrogen storage tanks because it has low susceptibility to hydrogen environment embrittlement (HEE) [2]. Unfortunately, solution-treated austenitic stainless steels have relatively lower yield strength compared to other types of stainless steels which results in high wall thickness to withstand the operational stresses [3, 4]. The mechanical properties can be improved by cold work-hardening because of dislocation multiplication, twining and strain-induced martensitic transformation, while dislocation multiplication and twining are the only two strengthening mechanisms in stable austenitic stainless steels [5].

Many efforts have been made to clarify the effects of cold working on the HEE of austenitic stainless steels. Tsong-pyng et al. [6] reported that 80% cold deformation had little effect on the hydrogen diffusivity in AISI 310 stable austenitic stainless steel, while cold deformation increased the hydrogen diffusivity greatly due to strain-induced α' martensitic transformation in metastable austenitic stainless steels (AISI301, AISI304). Han [7] and Zhang [8] found that prestrain at low temperatures resulted in a large amount of α' martensite in metastable austenitic stainless. Moreover, that dynamic α' martensite plays a primary role in HEE of the prestrained austenitic steel [8]. The hydrogen effects on the static mechanical properties have been widely investigated [5-8], but the hydrogen induced degradation of fatigue properties of metallic materials is more critical in industry applications. Mine et al. [9] investigated the fatigue crack growth rate (FCGR) of thermal hydrogen-charged specimens with different degrees of pre-strain, and found that the coupled effect of strain-induced α' martensite and hydrogen induced fatigue crack growth. Kanezaki et al. [10] found that more α' martensite on the fatigue fracture surface formed in pre-strained SUS316 specimens than solution-treated SUS 316 specimens, indicating that the α' martensitic transformation is closely related to the deformation microstructure. The microstructure and texture evolution caused by cold deformation in metastable austenitic stainless steels had been studied in details by many researchers [11, 12]. Chowdhury et al. [11] reported that the texture induced by cold rolling were dependent on the composition and deformation temperature in face-centred cubic materials. It could be inferred that the microstructure of warm-rolled steels will be different with the cold-rolled steels. However, there are few reports on the evolution of the microstructure induced by warm-deforming and its effect on HEE during subsequent deformation.

The objectives of this study were to investigate the dependence of microstructure and texture of austenitic stainless steel on deformation temperature and strain, and the effect of warm-deformed microstructure on the fatigue crack growth rate (FCGR) in high-pressure hydrogen and argon gas environments. The α' martensitic transformation near the fatigue crack tip and its effect on HEE was also investigated.

2. MATERIALS AND EXPERIMENTAL METHOD

2.1 Materials

The materials used in this study were type 316 (AISI 316) austenitic stainless steel with the following composition (in mass %): 0.02 C, 0.56 Si, 1.17 Mn, 16.6 Cr, 10.2 Ni, Mo 2.13. δ-ferrite influences the fatigue growth rate and tensile properties in the hydrogen environment [13]. To eliminate the influence of δ-ferrite, the as-received 316 specimens were solution-treated at 1100℃ for 30min followed by water quenching. Fig. 2 (b) reveals the microstructure of the as-received specimen, it shows a microstructure of a recrystallized austenitic single structure with the mean grain size is

approximately 100 μm, and no δ-ferrite was found.

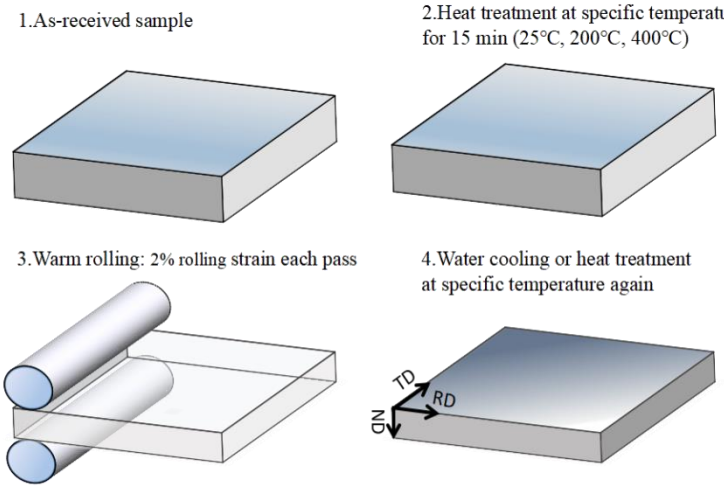

Figure 1. Schematic diagram of heat treatment and warm rolling process.

2.2 Specimens

The as-received 316 stainless steel plates were repeatedly rolled by a constant temperature rolling mill from 20mm thickness to obtain a specific thickness reduction (-0.2, -0.4), as shown in Fig. 1. It is necessary to avoid the sensitization effect which could increase the susceptible of austenitic stainless steels to intergranular corrosion and stress corrosion [14, 15]. Therefore, the rolling temperature was controlled below 500℃ (25℃, 200℃, 400℃). The thickness reduction was controlled roughly 2% each pass. In order to deform at a predetermined temperature, plates were heated in a muffle furnace for 15min or cooled by water between passes. Hereafter, the obtained strips will be called as TXX-RYY specimens, where the TXX -RYY means rolling to true stain YY at XX℃ (for example, T25-R20).

2.3 Experimental Method

The SSRT and FCG tests were performed using the Instron 8801 universal test system which was equipped with a high pressure gas environment chamber. Tensile test was conducted at a 5×10^{-5} s^{-1} strain rate in a 5MPa argon or hydrogen environment (99.999 % purity). The vacuuming and aeration processes were alternated three times to completely replace the gas adsorbed on the inner wall of the chamber, ensuring that the gas purity in the chamber meets the standard (ANSI/CSA CHMC-1) [16]. The 30 minutes pressure stabilization process was performed before each tensile or fatigue test. The elongation (δ) and engineering stress (σ) can be calculated by the following formulas: $\delta = L_F/L_0 - 1$ and $\sigma=P/A_0$, respectively. L_F and L_0 represent the initial and final gauge length, while P and A_0 represent load and initial cross-sectional areas, respectively. In addition, the load was measured with an external load cell compensated for seal friction. The FCGR test was conducted with compliance method, using the Instron 8801 universal test system under a 5 MPa argon or hydrogen atmosphere. The specific settings of the experimental parameters were as follows: force range ΔP = 5 kN, stress ratio R = 0.1, and testing frequency f = 1 Hz. All tests were performed at 25±2℃. To avoid accidental errors, all experiments were repeated three times. Using scanning electron microscopy (SEM) and electron back scattered diffraction (EBSD), the microstructure and phase structure of fracture surface and crack tip were studied.

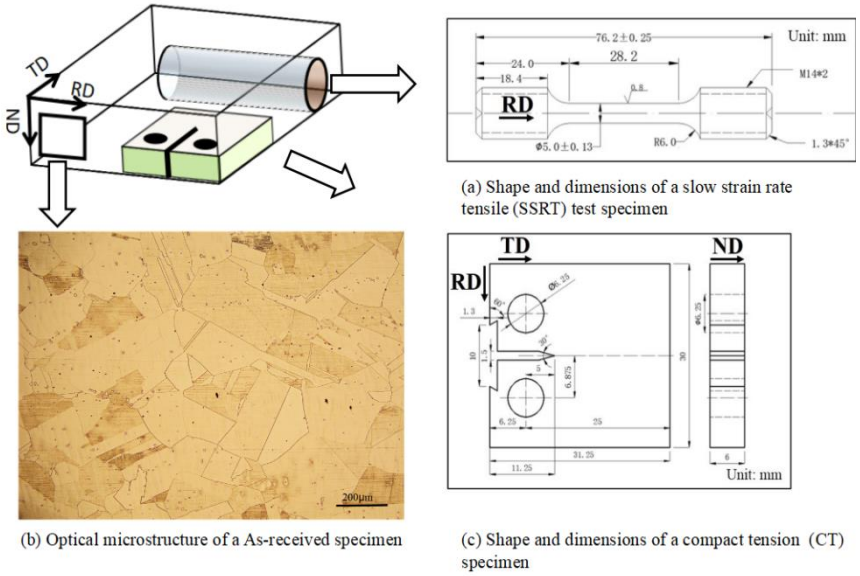

(a) Shape and dimensions of a slow strain rate tensile (SSRT) test specimen

(b) Optical microstructure of a As-received specimen

(c) Shape and dimensions of a compact tension (CT) specimen

Figure 2. Schematic diagrams of dimensions and orientation for the compact tension (CT) and the slow strain rate tensile (SSRT) specimens, and orientation for optical miscrotructure. Rolling direction (RD), normal direction (ND), and transverse direction (TD) are marked in the diagrams, respectively.

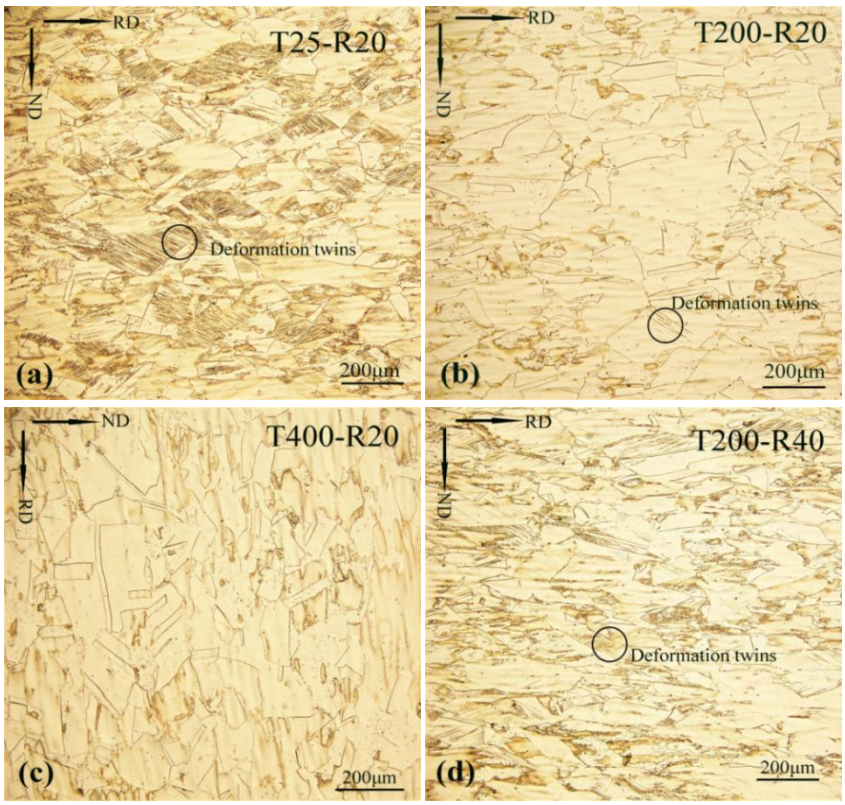

Figure 3. Dependence of optical microstructure on rolling strain or rolling temperature for the warm-rolled specimens.

3.EXPERIMENTAL RESULTS

3.1 Worm-Rolled Microstructure

The optical microscopy images of T25-R20, T200-R20, T400-R20 and T200-R40 specimens are shown in Fig. 3. A large number of deformation twins were observed in T25-R20 and T200-R40 samples after rolling in Fig. 3 (a) and (d), while the amount of deformation twins was smaller in the T200-R20 sample in Fig.3 (b). However, no deformation twin was found in the T400-R20 sample in Fig. 3 (c). Olson et al. [17] reported that the temperature dependence of the formation of deformation twins, it is easier to form twins when deforming at low temperatures. Tsakiris et al. [18] also reported that the proportion of twins determined by the strain degree. The deformation mechanism is mainly twining at low temperature but shifts to dislocation slip at higher temperature. Otherwise, dislocation slip was blocked due to piling up of dislocations with the increase of stain, twining happened again. Comparing Fig. 3 (a) with Fig. 3 (d), the grains were elongated along the rolling direction and the orientation of the deformation twins were gradually parallel to the rolling direction with the increase of rolling strain.

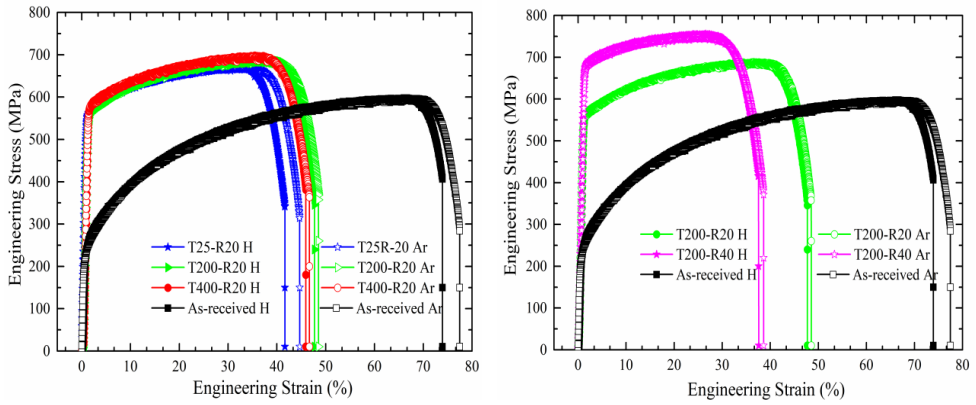

Figure 4. Dependence of stress–strain curves on rolling temperature (a) or rolling strain (b) for the as-received and warm-rolled 316 SSRT specimens tested in 5 MPa argon or hydrogen gases.

3.2 Slow Strain Rate Tensile Test

Fig. 4 (a) and Fig. 4 (b) shows the effects of rolling temperature and rolling strain on the stress–strain curves of as-received and warm-rolled 316 specimens. All samples tested in a hydrogen environment were named with TXX-RYY H_2 and marked with solid symbols in the Fig. 4 (a) and (b). All samples tested in argon were named with TXX-RYY Ar and marked with hollow symbols. The elongation of the specimen tested in argon was slightly higher than that of the specimen tested in hydrogen to the same rolling condition, and the difference in elongation diminished after warm rolling. From Fig. 4, hydrogen had little effect on the tensile curve before necking. The rolling temperature had little effect on the yield strength (YS) and ultimate tensile strength (UTS), while the elongation first increased and then decreased with increasing rolling temperature, as shown in Fig. 4 (a). The UTS and YS increased, but the elongation decreased with increasing rolling strain as shown in Fig. 4 (b). Nevertheless, the change magnitude in UTS, YS and elongation decreased with increasing strain.

3.3 Fatigue Crack Growth

Fig. 5 (a) shows the effect of rolling temperature on the FCGRs of as-received and warm-rolled 316 specimens tested in 5 MPa argon or hydrogen gases. All specimens tested in argon gas showed much lower fatigue growth rate than those tested in hydrogen gas, which indicates that hydrogen

enhances fatigue crack propagation. Compared with the as-received specimen, the FGGRs of worm-rolled specimens in both hydrogen and argon gases decreased significantly, which implies that the deformation structure induced by warm-rolling might decrease the FCGRs. The FGGRs of the specimens with different rolling temperatures represented the similar evolution trend in argon gas. An interesting result was found by comparing the curves of T400-R20 H_2, T200-R20 H_2 and T25-R20 H_2. The curves of T25-R20 H_2 and T200-R20 H_2 were almost identical, while the FGGR of T400-R20 H_2 showed an obvious difference. At low ΔK values, the T400-R20 H_2 specimen had a higher FCGR than the other two specimens. Above 40 MPa·m$^{0.5}$ ΔK, the FGGR of T400-R20 H_2 gradually became lower than those of the other two specimens.

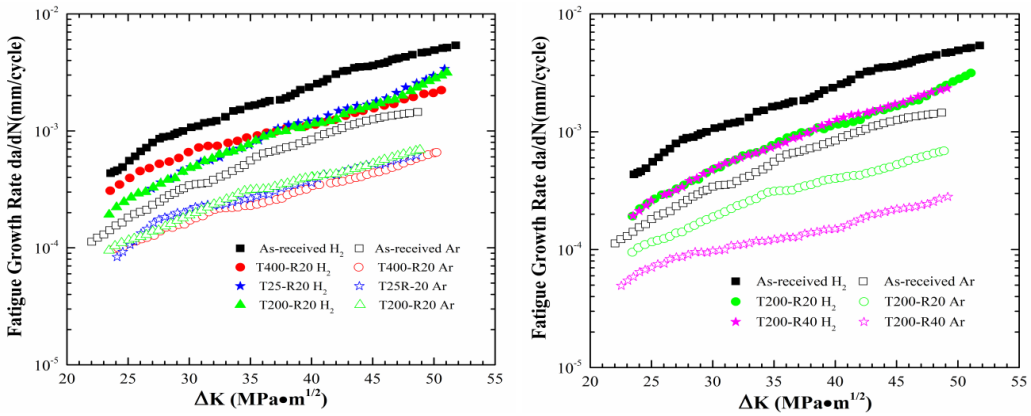

Figure 5. Dependence of FCGRs on rolling temperature (a) or rolling strain (b) for the as-received and warm-rolled 316 CT specimens tested in 5 MPa argon or hydrogen gases.

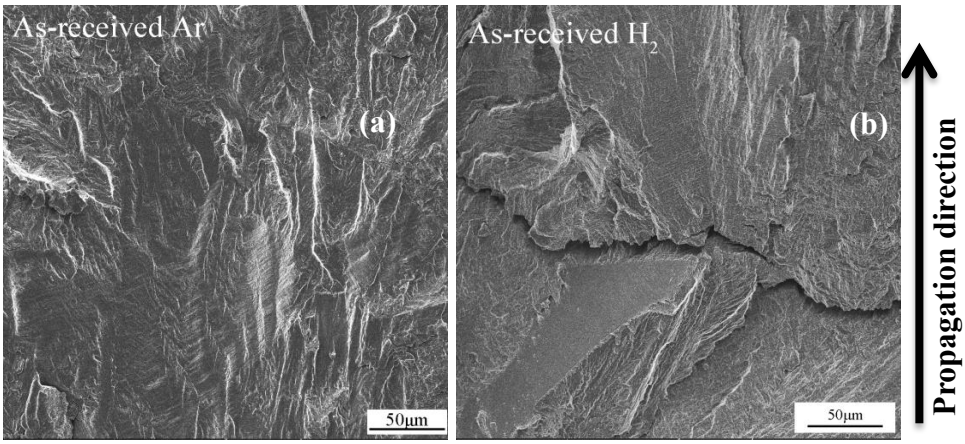

Figure 6. SEM fracture surface morphologies (near 40 MPa·m$^{0.5}$ ΔK) of as-received CT specimens tested in 5 MPa argon or hydrogen gases.

Fig. 5 (b) shows the effect of rolling strain on the FCGRs of as-received and warm-rolled 316 specimens tested in 5 MPa argon or hydrogen gases. The FCGRs of the specimens tested in hydrogen and argon showed different dependences on the rolling strain. The rolling strain had little effect on the FCGRs tested in hydrogen gas, while it influenced the FCGRs tested in argon gas greatly, namely, the FCGRs decreased with increasing the rolling strain in argon gas.

Fig. 6 shows the SEM fractographs of as-received 316 CT specimens tested in hydrogen and argon gas environments. The ΔK values corresponding to the stress and strain state near the crack tip has an effect on the fracture surface morphologies [18]. Thus, all SEM fractographs in this study were observed near 40 MPa·m$^{0.5}$ ΔK. The morphology of ductile fracture was found in the as-received 316

specimen tested in argon gas, while the quasi-cleavage fracture surface and a secondary crack were observed in the as-received 316 specimen tested in hydrogen gas. Fig. 7 shows the effects of rolling temperature and rolling strain on fracture surface morphologies of warm-rolled 316 specimens tested in argon gas and hydrogen gas. The ductile transgranular fracture surface with some stripes parallel to the crack propagation direction was clearly seen in those specimens tested in argon gas. The rolling temperature has little effect on the fracture surface morphologies. In addition, it was found that the spacing between the stripes gradually decreased with increasing rolling strain. To the specimens tested in hydrogen gas, the transgranular fracture surface with step-like features was observed in the low temperature rolling specimens (T25-R20 H_2 T200-R20 H_2 T200-R40 H_2), and the step-like features became more disorganized and multidirectional with increasing rolling strain. Furthermore, the step-like structure formed by low temperature rolling was replaced by the fracture surface with stripe-like fractures in the T400-R20 H2 specimen.

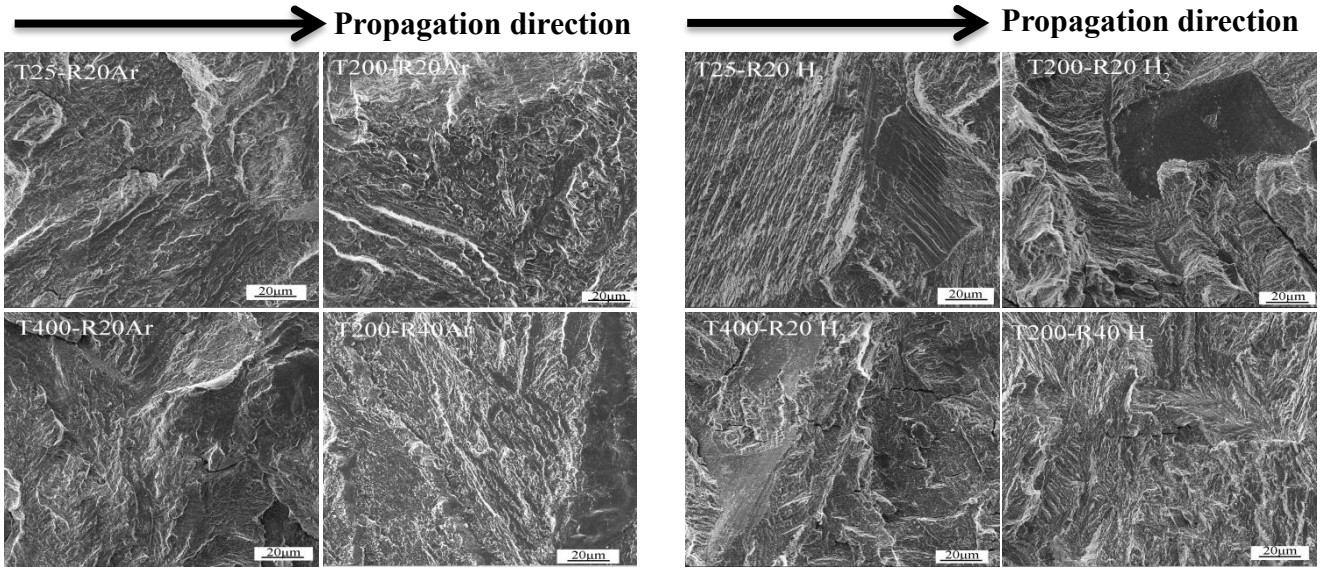

Figure 7. Dependence of SEM fracture surface morphologies (near 40 MPa·m$^{0.5}$ ΔK) on rolling temperature or rolling strain for the warm-deformed 316 CT specimens tested.

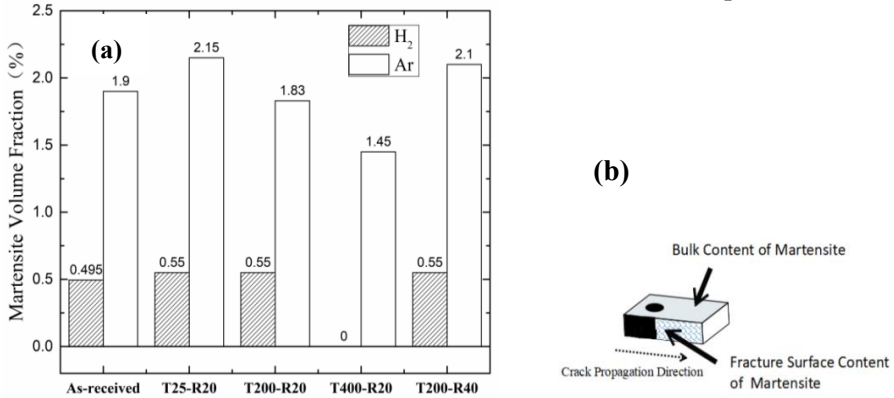

Figure 8. Schematic diagrams of the α′-matensite volume fractions on the fracture surface (near 40 MPa·m$^{0.5}$ ΔK) (a) and test method (b).

Fig. 8 shows the α′-matensite volume fractions on the fracture surface (near 40 MPa·m$^{0.5}$ ΔK) tested in argon and hydrogen gas. The contents of α′-martensite in various specimens were measured by the Ferritescope which measures the volume fraction of α′ martensite yielding from the detected site [20].

The true α′ martensite content (C_T) induced by cyclic deformation was calculated by the following formula:

$$C_T = C_F - C_B \quad (1)$$

where C_T – α′ martensite content induced by cyclic deformation, %; C_F – α′ martensite content of fracture surface, %; C_B – α′ martensite content of bulk.

It is clear that the α' martensite content tested in argon gas was much higher than that tested in hydrogen gas to the specimens with the same rolling condition. The value of C_T in the T400-R20 H_2 specimen was zero, and this indicated that no α' martensite formed in the vicinity of the crack during the fatigue crack propagation. In addition, the specimens rolled at lower temperatures (T25-R20 H_2, T200-R20 H_2 and T200-R40 H_2) had almost the same α′ martensite content in the vicinity of the crack, which implied that the strain level at lower rolling temperatures might have little effect on the content of α′ martensite in the vicinity of the crack.

4.DISCUSSION

The FCGRs of 316 austenitic steel were mainly affected by three factors: stress intensity at crack tip, microstructure, and test environment. And these three factors were not independent on each other. For example, plastic deformation was more severe at the crack tip with higher stress intensity, which means higher dislocation density and higher stress-induced α' martensite content in this region. Therefore, in order to understand the propagation process of fatigue cracks, it is important to clarify the deformation structure of 316 stainless steel specimens after warm rolling. Dislocations, α' martensite, and twins were likely to be induced by warm-rolling. Many studies on cold-deformed austenitic stainless steels have shown a close relationship between deformation microstructure and deformation temperature or deformation strains [29]. The most typical temperature dependent deformation microstructure is α' martensite. M_{d30} is a widely used index to measure the inclination of martensitic transformation in austenitic metals. The M_{d30} values of 316 austenitic steel used in this study were calculated with Angel's equation [30],

$$M_{d30}(℃) = 413\text{-}462([C] + [N]) - 9.2[Si] - 8.1[Mn] - 1.37[Cr] - 9.5[Ni] - 1.85[Mo] \quad (2)$$

The calculated result is much lower than the rolling temperatures, which indicates that almost no α' martensitic transformation occurs during warm rolling. This conclusion can also be proved by the value of bulk α' martensite content (C_B) for all samples being approximately 0.08%. Therefore, dislocation multiplication and twining are the only two deformation mechanisms in the worm-rolled 316 specimens. The deformation mechanism is mainly twining at low temperatures, but shifts to dislocation slip at higher temperatures in warm-rolled specimens with 20% thickness reduction (as mentioned in Section 3.1). And the volume fraction of them both increased with strain.

It is because of the microstructure change caused by warm rolling that the FCGRs of different specimens have changed. The warm-rolled specimens showed the obvious reduction in the FCGRs compared to the as-received specimens, which can be attributed to the increase in yield strength caused by warm rolling. As a result, the plastic zone near the fatigue crack tip will shrink. Tao [24] and Shrinivas [25] reported the relationship between the plasticity size and FCGR. The effect of yield strength was more pronounced to the specimens tested in argon gas; thus the FCGRs decreased with increasing rolling strain. The rolling temperature had little effect on yield strength from Fig. 4 (a); thus

the rolling temperature didn't almost affect the FCGRs of the specimens tested in argon. To the specimens tested in hydrogen gas, the mechanism of fatigue crack propagation becomes more complicated due to the coupling effect of high-pressure hydrogen, triaxial stress and microstructure. In general, the accumulation of hydrogen promotes plastic deformation near the crack tip, which results in the higher FCGR of the specimen tested in hydrogen gas. In detail, the slope of the FCGR curve tested in hydrogen gas showed a downward trend as the rolling temperature increased, especially the curve of the T400-R20 H_2 specimen in Fig. 5 (a). In contrast, the rolling strain seems to have little effect on the FCGR of the specimen tested in the hydrogen gas.

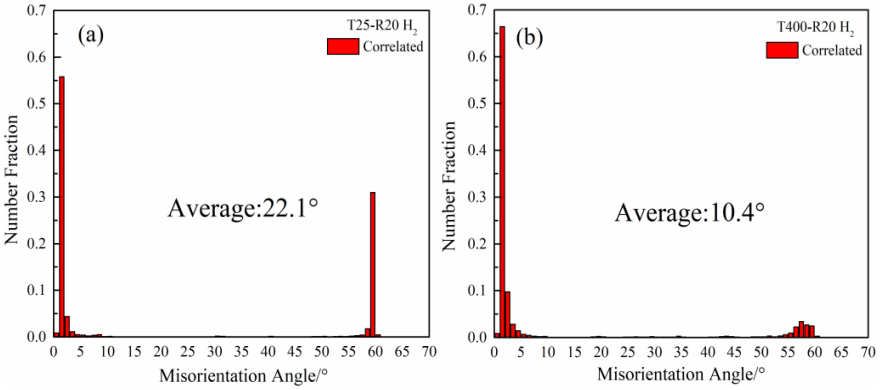

Figure.9 Misorientation angle distributions near the crack of warm-rolled 316 specimens (a) T25-R20 H_2 and (b) T400-R20 H_2.

Fig. 9 shows the misorientation angle distribution near the crack of warm-rolled 316 specimens (a) T25-R20 H_2 and (b) T400-R20 H_2. It can be observed that there are two distinct peaks around 3° and 60°, which represent dislocation and deformation twins, respectively. The fraction of deformation twins dramatically decrease from 0.3 to 0.03, while the dislocation fraction increase from 0.6 to 0.8 with rolling temperature. Both dislocation and deformation twins play the important roles in HEE of the austenitic stainless steels [6, 28]. As for dislocation，hydrogen is transported by dislocations [19] and reduces the repulsion between dislocations [20]. Low temperature deformation causes dislocation planar-slip and localized distribution of dislocation, but high temperature deformation causes dislocation cross-slip and uniform distribution of dislocation. As a result, the high density uniform distribution dislocation formed in T400R-20 H_2 transported sufficient quantities hydrogen over sufficient distances at earlier stages resulting in premature failure[5]. Thus, this may be the reason that the FCGR curve of the T400-R20 H_2 specimen was higher than that of the T25-R20 H_2 specimen below 40 $MPa{\cdot}m^{0.5}$ ΔK. As for deformation twins, it have little effect on HEE of austenitic steel compared with α' martensite and dislocation. However, the volume fraction of deformation twins greatly influences the content of α' martensite induced by cyclic deformation near the crack tip. Nakada [21] reported that α' martensite preferentially nucleated at the twin boundary in 316 cold-rolled specimens because deformed twins and austenite grains together form a double Kurdjumov–Sachs (K–S) relationship. Shen [22] found that α' martensite preferentially nucleated on the intersection of twins. It was well discussed that the higher hydrogen diffusivity and the lower hydrogen solubility of the α' martensite compared to the austenite leads to critical hydrogen concentrations at shorter times resulting in a high FGGR [25, 2 6].

The phase map (red for α' martensite phase and blue for austenite phase) and inverse pole figure (IPF) of T400-R20 H_2 and T25-R20 H_2 316 CT specimens near the crack tip are shown in Fig.10. Almost no α' martensite was observed in the plastic region near the crack in the T400-R20 H_2

specimen, while the austenite phase was completely transformed to α' martensite in the vicinity of the crack in the T25-R20 H_2 specimen. α' martensite nucleates and grows preferentially at the interface between deformation twin and austenite. Due to the preferential nucleation of α' martensite at the twin boundary, the fatigue crack propagates preferentially along the twin boundary. As a result, the step-like

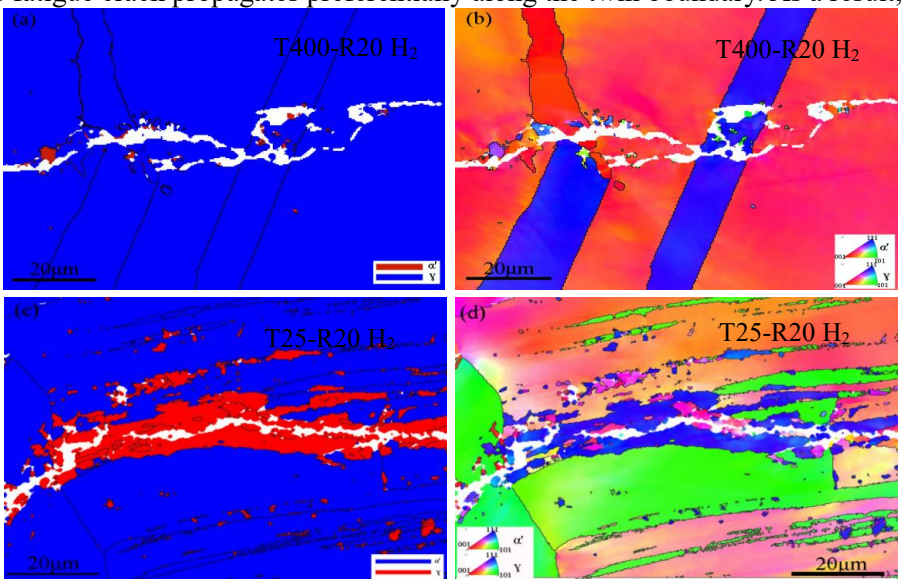

Figure 10. Phase diagram (a), (c) and inverse pole figure (IPF) map (b), (d) near the crack of worm-rolled 316 specimens T400-R20 H_2 and T25-R20 H_2.

twin structures appeared on the fracture surface of the specimen tested in hydrogen gas, as shown in Fig. 7. The FCGR of the T400-R20 H_2 specimen is gradually lower than the T200-R20 H_2 specimen above 40 MPa·$m^{0.5}$ ΔK, which indicates that the role of deformation twins on the FCGR becomes more important with the increase of the ΔK value. From mentioned above, warm rolling can improve the microstructure of dislocations and deformation twins, and then inhibit the formation of α' martensite, which is favorable to reduce the FCGR in hydrogen gas environment. Therefore, warm rolling takes both strength and hydrogen embrittlement into account, and improves the hydrogen embrittlement resistance of austenitic stainless steels on the basis of high strength.

5.CONCLUSION

The effect of warm-rolling on the FCGR of type 316 austenitic steel was investigated in 5 MPa argon gas and hydrogen gas. The main conclusions are as follows:

1. Warm rolling improved the strength, but did not increase the hydrogen embrittlement susceptibility. The fatigue crack growth rates (FCGR) of warm-rolled 316 specimens tested in hydrogen decreased with increasing rolling temperature, especially 400°C rolling.
2. The deformation microstructure of type 316 steel strongly depends on the rolling temperature. The amount of deformation twins decreased with increasing rolling temperature and twining was completely suppressed at 400°C.
3. Warm rolling can improve the microstructure of dislocations and deformation twins, and then inhibit the formation of α' martensite, which is favorable to reduce the FCGR in hydrogen gas environment. Warm rolling improves the hydrogen embrittlement resistance of austenitic stainless steels on the basis of high strength.

ACKNOWLEDGEMENTS

This research was supported by the National Key Basic Research Program of China (973 Program, Grant No. 2015CB057601), the National Natural Science Foundation of China (51571181) and the Zhejiang Provincial Natural Science Foundation of China (LY19E010006).

REFERENCES

1. Murakami, Y., and Ritchie, R.O., 11 – Effects Of Hydrogen On Fatigue-Crack Propagation In Steels. *Gaseous Hydrogen Embrittlement of Materials in Energy Technologies* **17,** No. 4, 2012, pp. 379-417.
2. Marchi, C., San, et al. On the Physical Differences Between Tensile Testing of Type 304 And 316 Austenitic Stainless Steels with Internal Hydrogen and In External Hydrogen. *International Journal of Hydrogen Energy* **35,** No. 18, 2010, pp. 9736-9745.
3. Marshal, P., Austenitic Stainless Steel: Microstructure and Mechanical Properties, 1st ed, Elsevier Science Publishing, New York 1984, p.80.
4. Washko, S. D., and Aggen, G., ASM Handbook Vol 1: Properties And Selection, 3rd ed, ASM International, New York, 2005, p. 1303.
5. Michler, T., Naumann, J., Hock, M., Microstructural Properties Controlling Hydrogen Environment Embrittlement of Cold Worked 316 Type Austenitic Stainless Steels. *Materials Science & Engineering A*, **628**, 2015, pp. 252-261.
6. Tsongpyng, P., Altstetter, C. J., Effects of Deformation on Hydrogen Permeation in Austenitic Stainless Steels. *Acta Metallurgica*, **34,** No. 9, 1986, pp. 1771-1781.
7. Han, G., He, J., Fukuyama, S., Effect of Strain-Induced Martensite on Hydrogen Environment Embrittlement of Sensitized Austenitic Stainless Steels at Low Temperatures. *Acta Materialia*, **46**, No.13, 1998, pp. 4559-4570.
8. Zhang, L., Li, Z., Zheng, J., Influence of Low Temperature Prestrain on Hydrogen Gas Embrittlement of Metastable Austenitic Stainless Steels. *International Journal of Hydrogen Energy*, **38**, No. 25, 2013, pp. 11181-11187.
9. Mine, Y., Narazaki, C., Murakami, K., et al. Hydrogen Transport in Solution-Treated and Pre-Strained Austenitic Stainless Steels and Its Role in Hydrogen-Enhanced Fatigue Crack Growth. *International Journal of Hydrogen Energy*, **34**, No. 2, 2009, pp. 1097-1107.
10. Kanezaki, T., Mine, Y., Matsuoka, S., Effects of Hydrogen on Fatigue Crack Growth Behavior of Austenitic Stainless Steels. *International Journal of Hydrogen Energy*, **33,** No. 10, 2008, pp. 2604-2619.
11. Chowdhury, S. G., Das, S., De, P. K., Cold Rolling Behaviour and Textural Evolution in AISI 316L Austenitic Stainless Steel. *Acta Materialia,* **53**, No. 14, 2005, pp. 3951-3959.
12. Raabe, D., Texture and Microstructure Evolution During Cold Rolling of a Strip Cast and of a Hot Rolled Austenitic Stainless Steel. *Acta Materialia*, **45**, No. 3, 1997, pp. 1137-1151.
13. Buckley, J. R., Hardie, D., The Effect of Pre-Straining and δ-Ferrite on The Embrittlement of 304L Stainless Steel by Hydrogen. *Corrosion Science*, **34**, No. 1, 1993, pp. 93-107.
14. Tsay, L. W., Liua, Y. F., Huang, R. T., et al. The Effect of Sensitization on The Hydrogen-Enhanced Fatigue Crack Growth of Two Austenitic Stainless Steels. *Corrosion Science*, **50**, No. 5, 2008, pp.

0-1367.

15. Purtscher, P. T., Quantifying The Embrittlement Due to Sensitization in An Austenitic Stainless Steel. *Scripta Metallurgica Et Materialia*, **26,** No. 3, 1992, pp. 343-346.
16. American National Standard Institute. Test Methods for Evaluating Material Compatibility in Compressed Hydrogen Applications Metals. ANSI/CSA CHMC 2014;1.
17. Olson, G. B., Cohen, M., Kinetics of Strain-Induced Martensitic Nucleation. *Metallurgical Transactions A*, **6**, No. 4, 1975, p. 791.
18. Tsakiris, V., Edmonds, D. V., Martensite and Deformation Twinning in Austenitic Steels. Materials Science & Engineering A (Structural Materials:, Properties, Microstructure and Processing), 273-275(none), 1999, pp. 430-436.
19. Matsunaga, H., Noda, H., Visualization Of Hydrogen Diffusion in a Hydrogen-Enhanced Fatigue Crack Growth in Type 304 Stainless Steel. *Metallurgical & Materials Transactions A*, **42**, NO. 9, 2011, pp. 2696-2705.
20. Chen, T. C., Chen, S. T., Tsay, L. W., The Role of Induced α′-Martensite on The Hydrogen-Assisted Fatigue Crack Growth of Austenitic Stainless Steels. *International Journal of Hydrogen Energy,* **39,** No. 19, 2014, pp. 10293-10302.
21. Nakada, N., Ito, H., Matsuoka, Y., et al. Deformation-Induced Martensitic Transformation Behavior in Cold-Rolled and Cold-Drawn Type 316 Stainless Steels. *Acta Materialia*, **58**, No. 3, 2010, pp. 895-903.
22. Shen, Y. F., Li, X. X., Sun, X., et al. Twinning And Martensite in a 304 Austenitic Stainless Steel. *Materials Science and Engineering A*, **552**, No.34, 2012, pp. 514-552.
23. Entwisle, A. R., The Kinetics of Martensite Formation in Steel. *Metallurgical Transactions*, **2,** No.9, 1971, pp. 2395-2407.
24. Tao, H., Hong, Y., Chen, X., et al. Hydrogen Effect on The Fatigue Crack Growth in Austenitic Stainless Steel Investigated by a New Method Based on Nanohardness Distribution. *Journal Of Materials Engineering And Performance,* **27**, No.12 2018, pp. 6485-6492
25. Shrinivas, V., Varma, S. K., Murr, L. E., Deformation-Induced Martensitic Characteristics in 304 and 316 Stainless Steels during Room-Temperature Rolling. *Metallurgical and Materials Transactions A,* **25**, No.3, 1995, pp. 661-671.
26. Murakami, Y., Kanezaki, T., Mine, Y., et al. Hydrogen Embrittlement Mechanism in Fatigue of Austenitic Stainless Steels. *Metallurgical and Materials Transactions A (Physical Metallurgy and Materials Science)*, **39**, No. 6, 2008, pp. 1327-1339.
27. Rozenak. P., Robertson, I. M., Birnbaum, H. K., HVEM Studies of The Effects of Hydrogen on The Deformation and Fracture of AISI Type 316 Austenitic Stainless Steel. *Acta Metallurgica et Materialia,* **38** , No. 11, 1990, pp. 2031-2040.
28. CHATEAU, J. P., DELAFOSSE, et al. Numerical Simulations of Hydrogen-Dislocation Interactions in Fcc Stainless Steels. Part I: Hydrogen-Dislocation Interactions in Bulk Crystals. *Acta Materialia*, **50,** No. 6, 2002, pp. 1523-1538.
29. Dowling, N. E., Mechanical Behavior of Materials / Engineering Methods for Deformation, Fracture, And Fatigue. *International Journal of Fatigue*, **19**, No. 96, 1999, p. 85.
30. Angel, T., Formation of Martensite in Austenitic Stainless Steels – Effects Of Deformation, Temperature and Composition. *Iron Steel Inst*, **177**, 1954, pp. 1650-174.